REVIEW

Six-Coordinated Co^{II} Single-Molecule Magnets: Synthetic Strategy, Structure and Magnetic Properties

Mengmeng Wang,[a,b] Zongsu Han,[b,c] Yann Garcia,*[a] Peng Cheng*[b]

[a] Dr. M. Wang, Prof. Dr. Y. Garcia
Institute of Condensed Matter and Nanosciences, Molecular Chemistry, Materials and Catalysis (IMCN/MOST), Université catholique de Louvain, 1348 Louvain-la-Neuve, Belgium.
E-mail: yann.garcia@uclouvain.be; pcheng@nankai.edu.cn
[b] Dr. M. Wang, Dr. Z. Han, Prof. Dr. P. Cheng
Key Laboratory of Advanced Energy Materials Chemistry (MOE) and Frontiers Science Center for New Organic Matter, College of Chemistry, Nankai University, Tianjin 300071, China.
[c] Dr. Z. Han
Department of Chemistry, Texas A&M University, College Station, Texas 77843, United States.

Abstract: The pursuit of molecule-based magnetic memory materials contributes significantly to high-density information storage research in the frame of the ongoing information technologies revolution. Remarkable progress has been achieved in both transition metal (TM) and lanthanide based single-molecule magnets (SMMs). Notably, six-coordinated Co^{II} SMMs hold particular research significance owing to the economic and abundant nature of 3*d* TM ions compared to lanthanide ions, the substantial spin-orbit coupling of Co^{II} ions, the potential for precise control over coordination geometry, and the air-stability of coordination-saturated structures. In this review, we will summarize the progress made in six-coordinated Co^{II} SMMs, organized by their coordination geometry and molecular structure similarity. Valuable insights, principles, and new mechanism gleaned from this research and remaining issues that need to be addressed will also be discussed to guide future optimization.

1. Introduction

The evolution of information technology and the shrinking size of electronic devices have pushed traditional magnetic materials to their storage capacity limits. The concept of encoding binary information into a single molecule offers a promising avenue to significantly increase data storage density. The discovery of magnetization relaxation effect in complex $[Mn_{12}O_{12}(OAc)_{16}(H_2O)_4]\cdot 2AcOH\cdot 4H_2O$ brought hope to this concept and ignited research into a new class of material called single molecule magnets (SMMs).[1-3] To achieve practical applications, high blocking temperature (T_B, at which the magnetization is frozen) and long relaxation time (τ) are required. The establishment of high energy barrier to block magnetization reversal (U) is the first step towards accomplishing such requirements. For purely axial anisotropic spin systems, U is determined by the ground state spin value S and the uniaxial magnetic anisotropy. Hence, initial research focused on constructing giant-spin systems by assembling transition metal (TM) ions into clusters, which actually were found to reduce the magnetic anisotropy and led to negligible improvement in energy barrier.[4-6] Subsequent emphasis was placed on enhancing the magnetic anisotropy of mononuclear SMMs or so called as single-ion magnets (SIM) through ligand field optimization after the report of a mononuclear complex $[Pc_2Tb]^-$ with the highest effective energy barrier (U_{eff}) of 330.9 K in 2003.[7-13] Revolutionary strides have been made in recent years, exemplified by T_B reaching 80 K for $[(\eta^5\text{-}Cp^*)Dy(\eta^5\text{-}Cp^{iPr5})][B(C_6F_5)_4]$ and a coercive field (H_c) exceeding 14 T at temperatures below 60 K for $(Cp^{iPr5})_2Dy_2I_3$.[14,15] There are however still great challenges ahead considering the harsh synthesis conditions, air instability of this type of Ln-SMMs, and the limited availability and high cost of lanthanide ions.[16] Hence, seeking for cheaper and more abundant alternatives such as 3*d* TM ions as magnetic building units which would achieve excellent magnetic performances in stable complexes is needed. A renaissance in 3*d* TM based SIMs has been witnessed since the report of a linear Fe^I system with U_{eff} of 325 K in 2013.[17] Multifarious systems with interesting structures and properties as well as critical cognition about magnetic anisotropy and relaxation dynamics were achieved in the pursuit of enhancing U to give us more understanding towards the magneto-structural correlation.[18-23] Among 3*d* TM ions, Co^{II} ion stands out for assembling molecular nanomagnets due to its large magnetic anisotropy.[24-29] Various Co^{II} SIMs with coordination numbers ranging from 2 to 8 have been reported,[20,22] some exhibiting excellent performances, such as the two-coordinate linear Co^{II}-SIMs [(NHC)CoNDmp] and $[Co(C(SiMe_2Onaph)_3)_2]$ featuring high U_{eff} of 413 and 450 cm^{-1}, respectively.[30,31] However, to avoid air-sensitive complexes, research on saturated six-coordinated Co^{II} SMMs has increased considerably. Six-coordinated Co^{II} SMMs have coordination geometries varying from trigonal prism, trigonal antiprism to octahedron, which lead to different magnetic anisotropies, and different relaxation mechanisms. Furthermore, the prevailing under-barrier relaxation (relaxation that occurs at energies lower than that set by the magnetic anisotropy),[32-34] and relaxation originating from easy-plane magnetic anisotropy[35] have rich research values. Over years of development, systematic and important lessons can be summarized to guide future optimization. In this review, we will firstly briefly describe what is magnetic anisotropy, methods for obtaining magnetic anisotropy parameters and different relaxation processes. Then we shall summarize research progress on six-coordinated Co^{II} SMMs by sorting them based on the Co^{II} ion coordination geometry and structural similarity with particular focus on the correlation of coordination geometry with magnetic anisotropy and magnetization dynamics.

2. Theoretical Background

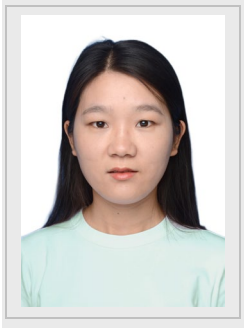

Mengmeng Wang received her Ph.D. degree in 2022 from Nankai University under the supervision of Prof. Peng Cheng and Prof. Wei Shi. Now she is working as a post doctor in Prof. Yann Garcia's group at Université catholique de Louvain, Belgium. Her current research interests focus on molecule-based magnetic materials (spin crossover materials and single-molecule magnets), and luminescent sensing materials.

Zongsu Han received his Ph.D. degree in 2022 from Nankai University under the supervision of Prof. Peng Cheng and Prof. Wei Shi. In 2019, he studied at the University of Manchester as a visiting student, under the supervision of Prof. Sihai Yang. Now he is working as a post doctor at Texas A & M University in Prof. Hong-Cai Zhou's group. His current research interests focus on the luminescent sensing materials.

Yann Garcia is a prof of analytical chemistry at UCLouvain. He has published more than 290 publications with several cover pages of top chemistry journals as well as a Wiley-VCH book on the chemical applications of Mössbauer spectroscopy. Along his various research projects, his group works on the design and applications of spin crossover materials. He is the current president of the GFSM Mössbauer society (gfsm.fr), and Vice chair of the IBAME society (ibame.org).

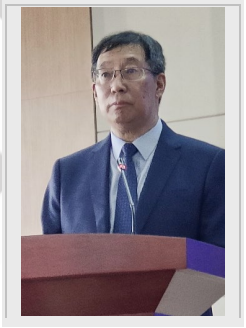

Peng Cheng is currently the Cheung Kong Professor at College of Chemistry, Nankai University, China. He received his BSc, MSc, and PhD from Nankai University in 1985, 1991, and 1994, respectively. Subsequently, he started his academic career at the same university and was appointed a full professor in 1996. From 1997 to 1999, he worked at Laboratoire de Chimie de Coordination du CNRS as a visiting professor and at Texas A&M University as a postdoctoral research fellow. His current research works focus on functional coordination polymers and molecule-based materials.

2.1. Magnetic Anisotropy

Magnetic anisotropy means the preferential alignment of the magnetic moment within a molecule along a specific direction, which is the origin of an energy barrier that blocks the magnetization from reorienting after removing the external magnetic field.[36] When the magnetic moment exhibits only two stable and antiparallel orientations (usually along the *z*-axis), the system is classified as having easy-axis magnetic anisotropy.[37] Conversely, when the magnetic moment is confined to a plane perpendicular to the *z*-axis, the system is categorized as having easy-plane anisotropy. Magnetic anisotropy can be represented by zero-field splitting (ZFS), which is the splitting of energy levels (M_S microstates) when the external magnetic field is zero under the synergistic effect of spin-orbit coupling and metal ion coordination environmental distortion.[38] *D* and *E* are defined to represent the axial and rhombic/transverse ZFS parameters with the related Hamiltonian expressed as:

$$\hat{H} = D[\hat{S}_z^2 - S(S+1)/3] + E(\hat{S}_x^2 - \hat{S}_y^2)$$

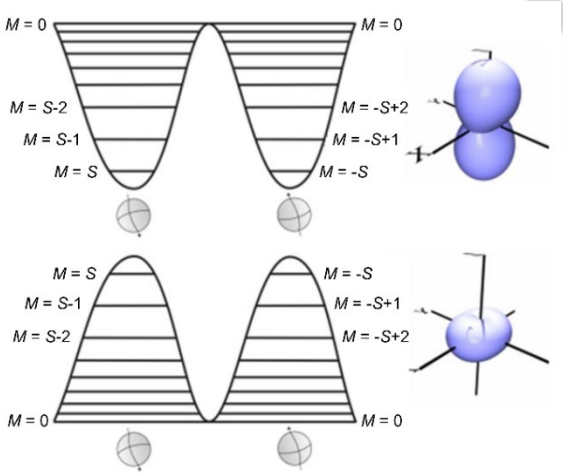

Figure 1. Double-well potential of easy-axis (upper) and easy-plane (down) anisotropy. Reproduced with permission from Ref. [36].

The operator $\hat{S}$ describes spin projection along a specific axis.[39] The parameter *D* can take positive or negative values, which influences the relative distribution of the M_S microstates according to the above ZFS Hamiltonian.[38] As illustrated in Fig. 1, when $D < 0$, the energy level with the largest M_S value is lower than those of the smaller M_S states, indicating that the orbital along the *z*-axis is lower in energy and the system has easy-axis anisotropy. On the contrary, when $D > 0$, the smallest M_S state has lower energy compared to larger M_S states, the orbital in the *xy*-plane has the lowest energy, and the system has easy-plane anisotropy (the notation M_S is used when the orbital angular momentum is largely quenched while M_J is used when the orbital angular momentum is significant).[36,40] For strictly axial anisotropic 3*d* spin systems, the energy barrier to block magnetization reversal *U* is associated with the energy level difference between the largest M_S and $M_S = 0$ with $U = |D|S^2$ and $U = |D|(S^2-1/4)$ for integer and non-integer spin systems, respectively, derived from the above spin Hamiltonian (the term 1/4 is introduced as a correction for different quantum tunneling effect and ZFS behave of integer and non-integer spin systems).[2,41,42] The magnetic anisotropy, energy level diagram, as well as value of magnetic anisotropy parameters and energy barrier to magnetization reversal depends on the interaction of metal ion and its coordination environment in coordination complexes. There are several methods to access the magnetic anisotropy parameters. The mostly used one is fitting from the magnetic measurements, including direct current (dc) susceptibility and variable field magnetization at low temperature.[43-45] However, these methods may not always provide accurate values due to the insensitivity of the

experimental data to the sign and sometimes the magnitude of *D*. For more reliable ZFS parameters, characterization techniques such as high-field, high-frequency electron paramagnetic resonance spectroscopy (EPR), nuclear magnetic resonance (NMR) paramagnetic shift, variable field THz spectroscopy, inelastic neutron scattering (INS), far-IR spectroscopy, and torque magnetometry studies can be conducted.[22,46-48] Additionally, theoretical approaches based on wavefunction techniques, such as SA-CASSCF, CASSCF/NEVPT2/CASPT2/MRCI/DMRG and DFT methods, can provide reliable estimates of these parameters.[49,50]

2.2. Slow Magnetization Relaxation

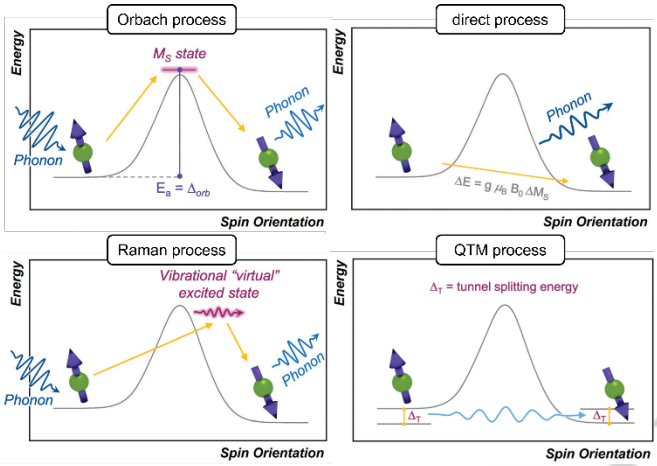

Figure 2. Schematic representation of Orbach, direct, Raman and QTM magnetization relaxation mechanisms. Reproduced with permission from Ref. [51].

Magnetic relaxation in SMMs refers to the process that the molecule's magnetic moment flips its magnetization orientation after removing the external magnetic field.[51] Ideally, in an SMM with an established *U*, magnetization reorientation should occur via the highest excited states assisted by thermal energy of the system (k_BT). However, owing to the quantum nature of molecular nanomagnets, relaxation mechanisms are intricate, varied, and sensitive to multiple factors. The most common magnetic relaxation processes in SMMs include Orbach, Raman, direct and quantum tunneling of the magnetization (QTM, Fig. 2). In the first three processes, the magnetic moments exchange energy with the lattice, termed as spin-lattice relaxation.[3] In Orbach process, a spin absorbs phonons from the lattice to transition from the ground to the highest excited sublevel and then release phonons to return to the ground sublevel with reversed magnetization orientation. The energy of the phonons must match the energy level difference between ground and excited sublevels. Hence, Orbach process usually occurs at high temperature due to the requirement of phonons with sufficient energy. Raman process, although also involving the absorption and release of phonons, proceeds through a virtual excited state, thus imposing less stringent energy restrictions compared to the Orbach process. Direct process involves a single phonon emission, transitioning from one microstate to another. QTM occurs between the doubly degenerated $\pm M_S$ sublevels without absorption and release of energy and is usually prevailing at low temperatures. There is also another tunneling mechanism, named thermally assisted QTM, which has energy exchange with lattice. In this process, the spin absorbs phonons to promote from the ground state to a higher-energy excited M_S sublevel (below the highest excited state) and then tunnels to the opposite M_S level, followed by a final relax to complete reorientation. It behaves analogously to Orbach process, proceeding through lower excited states rather than the highest one, which generates an effective energy barrier, U_{eff}.[51] Generally, multiple relaxation processes occur simultaneously in a system, each dominant within different temperature ranges.[52] Ac magnetic susceptibility measurements serve as a crucial tool for analyzing the slow magnetization relaxation process, allowing extraction of the τ at different temperatures. By fitting the temperature-dependent τ ($\ln(\tau)$ vs. T^{-1}) using the equation provided, parameters related to different relaxation processes including U_{eff} can be derived.

$$\tau^{-1} = \tau_{QTM}^{-1} + AH^nT + CT^m + \tau_0^{-1} \exp(-U_{eff}/k_BT)$$

The equation's components correspond to QTM, direct, Raman, and Orbach processes, respectively.[53] The non-Orbach relaxation processes are also termed as under barrier relaxation, which reduce the U_{eff} and T_B of SMM and should be suppressed.[33,54] The relaxation process is influenced by several factors, including strength and symmetry of the ligand field, spin state, isotopic identity, hyperfine and intermolecular interactions, local magnetic species, temperature, magnetic field, and so on.[51] Understanding the relaxation mechanism is pivotal for optimizing SMM performance.

3. Six-Coordinated Co^{II} SMMs

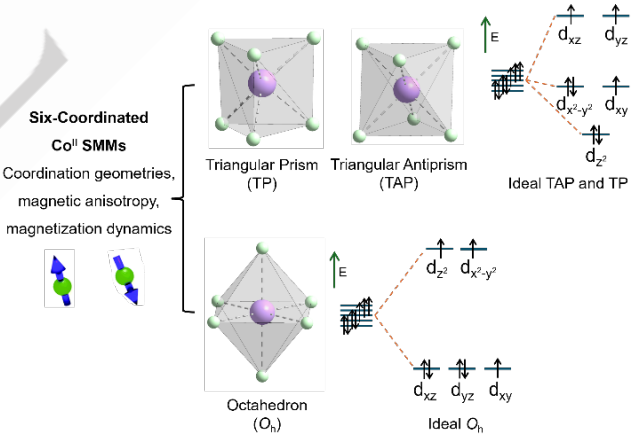

Scheme 1. Three ideal coordination geometries of six-coordinated Co^{II} SMMs: trigonal prism, trigonal antiprism, and octahedron, and their ideal *d* orbital splitting pattern for d^7 electronic configuration.

For TM ions, the crystal field strength outweighs spin-orbit coupling. Hence, the coordination field impacts electron level splitting significantly, making the rational design of ligand field crucial for TM based SMMs. In the case of six-coordinated Co^{II} SMMs, there are different coordination geometries on the Co^{II} ion. Quasi-octahedral configuration predominates due to the difficulty of experimentally realizing quasi-trigonal prismatic and quasi-trigonal antiprismatic configurations. Different coordination configurations, including different coordination geometries and type of coordinating atoms lead to different magnetic anisotropy

and magnetization dynamics. Additionally, the surrounding environment also affects the magnetic performance, which is complicated to analyze. Notably, octahedral Co^{II} SMMs may exhibit positive or negative *D* values in different cases, and new theories have been proposed to elucidate the slow magnetic relaxation behavior with easy-plane magnetic anisotropy.[35,55-57] Moreover, some rules are summarized between the structural distortion and magnetic property. Overall, the structure and properties of six-coordinated Co^{II} SMMS are highly diverse and multifaceted.

3.1. Trigonal Prismatic Coordination Geometry

3.1.1. CoN_6 Coordination Environment (Mononuclear)

The exploration of trigonal prism Co^{II} SMMs started from the theoretical calculation by Gomez-Coca *et al.* in 2013, which predicted the symbols of *D* of six-coordinate Co^{II} (*S* = 3/2) complexes to be negative in the trigonal prism coordination mode and having both possibilities in octahedral coordination mode depending on the distortion of the symmetry.[58] To validate this prediction, complex $[Co(P(S)\{[N(CH_3)NCHC_3N_2H_3]_3)\}](NO_3)_2$ (**1**, Fig. 3)[59] was studied, featuring a Co^{II} ion encapsulated by six N atoms in a trigonal prism coordination geometry. *D*(|*E*|) values of −72(7) cm^{-1} and −141(2.2) cm^{-1} were derived from dc magnetic data, and CASSCF-RASSI calculation, respectively. Under an applied magnetic field of 2000 Oe, slow magnetic relaxation was observed with U_{eff} of 23 cm^{-1}, representing the first example of trigonal prism mononuclear SMM. Since this kind of clathrochelate ligand has three arms, and on each arm, there are two coordination N atoms, which is perfect for encapsulating Co^{II} ion in trigonal prism coordination geometry, similar clathrochelate Co^{II} SMMs (**2**-**6**) have been reported with zero-field slow magnetic relaxation behavior (Fig. 3).[60-64]

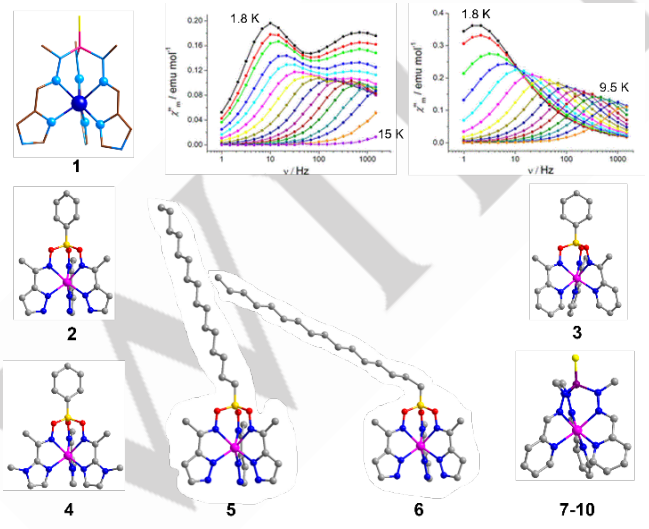

Figure 3. Top: Cationic structure of complex **1** (upper left) and its frequency dependence of χ'' under 375 Oe applied dc field (upper middle) and under 2000 Oe applied dc field (upper right). Down: molecular/cationic structures of corresponding Co^{II} clathrochelate SMMs. Reproduced with permission from Ref. [58].

Complexes $[Co(L^1)][CoCl_4]\cdot CH_3CN$ (**7**), $[Co(L^1)][ZnCl_4]\cdot CH_3OH$ (**8**), $[Co(L^1)]ClO_4\cdot 2CH_3OH$ (**9**), and $[Co(L^1)]BF_4$ (**10**, Fig. 3, L^1 = tris(pyridylhydrazonyl)phosphorylsulfide, (S)P[N(Me)N=C(H)Py]$_3$) employ a similar clathrochelate ligand, showcasing deviation values of Co^{II} ion coordination geometry towards trigonal prism of 3.839, 3.196, 3.002 and 2.759, respectively.[65] *D* values of −60.6 cm^{-1}, −87.2 cm^{-1}, −116.6 cm^{-1} and −127.6 cm^{-1} were deduced from dc magnetic measurements, with their absolute value decreases as distortion from trigonal prism to octahedron increases. No slow magnetic relaxation was observed in **7**, even under external dc fields, due to the short Co···Co distance leading to dipolar interactions that accelerates QTM. Complexes **8-10** exhibited SMM behavior under the corresponding optimal field with U_{eff} values of 24.0 cm^{-1} (2000 Oe), 26.8 cm^{-1} (1000 Oe), 27.2 cm^{-1} (2000 Oe), respectively. It is noteworthy that in the examples presented, the U_{eff} values were primarily obtained by fitting the high temperature linearity region in the ln(*τ*) vs. T^{-1} plot using the Arrhenius equation, and in most cases, these values are much lower than the theoretical activation energy of ~|2*D*|. Given that Orbach process proceeds through actual energy levels and no such low-energy level exists, relaxation should not occur via Orbach process. At high temperatures, Raman process was frequently revealed to dominate while QTM and/or direct processes preponderate at low temperatures.[32,33]

In addition to direct influences on the first coordination sphere, changes in the periphery groups distant from the metal center also significantly impact the magnetic property. Our group investigated the structure and diverse magnetization dynamics by modifying alkyl chains on Co^{II} acetylmethylimidazole-oximate complexes (non-alkyl substituted, methyl-, ethyl-, and *n*-propyl- substituted complexes, **11-14**) (Fig. 4).[66] The deviation values of coordination geometry towards trigonal prism are 0.786, 0.726, 0.653, and 0.685, respectively. Ac magnetic susceptibility measurements unveiled the remarkable influence of alkyl substitution on magnetization dynamics, manifesting in different relaxation rates at identical temperature, and faster QTM rate in the ethyl, and *n*-propyl substituted complexes, along with distinct relaxation processes. These variations in coordination geometry around the Co^{II} ion were deemed as a crucial factor for different magnetization dynamics by affecting the electron structure of Co^{II} ion and the contribution of transverse ZFS. Diverse crystal packings and potential variations in vibration modes induced by varying alkyl chains were hypothesized to impact relaxation processes by influencing dipolar magnetic interactions and rates of spin-flip via quantum tunneling. The observed slow magnetic relaxation was not attributed to Orbach process, as the U_{eff} values obtained, ranging from 14 K to 53 K are significantly lower than the calculated energy barrier of 286.0 cm^{-1} to 299.6 cm^{-1}.

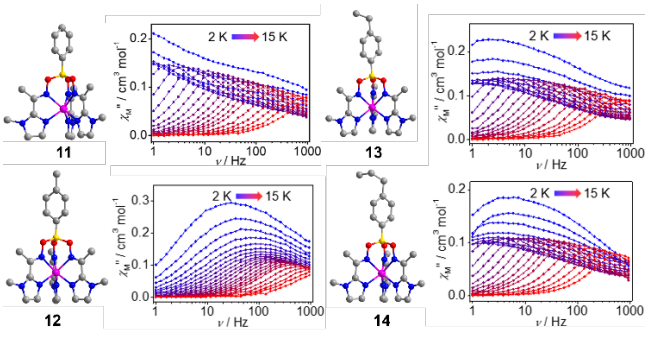

Figure 4. Cationic structures of complexes **11-14** and their frequency dependence of χ'' at zero dc field. Reproduced with permission from Ref. [66].

The metal salts $[L^2Co][CoCl_4]$ (**15**) and $\{Na[L^2Co]\}(BPh_4)_3$ (**16**, L^2 results from the reaction of one *cis*-,*cis*-1,3,5-triaminocyclohexane with three 2-formyl-5-(N-tert-butyl)-nicotinamide) adopt Co^{II} coordination geometries between trigonal prismatic and octahedral with torsion of the N–N–N planes about the 3-fold rotational axis of 23.3(1) and 15.8(7)°, respectively.[67] Magnetic susceptibility data fitting yielded D values of −11.0, and −75.8 cm^{-1} as well as $|E/D|$ of 0.00077, and 0.000012, respectively. Complex **15** does not exhibit slow relaxation of magnetization, even under an applied dc field, while **16** demonstrates slow magnetic relaxation at zero field with U_{eff} = 52.3 cm^{-1}.

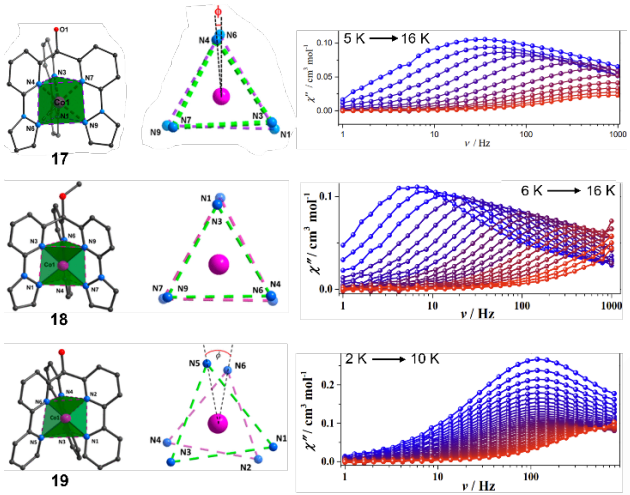

Figure 5. Cationic structures of complexes **17**-**19** (left) and their frequency dependence of χ'' at zero dc field (right). Reproduced with permission from Ref. [68,69].

Complexes $[Co(tppm)](ClO_4)_2{\cdot}2CH_3CN{\cdot}H_2O$ (**17**, tppm = tris[6-(1H-pyrazol-1-yl)pyridin-2-yl]methanol),[68] $[Co(tppm^*)](BPh_4)_2$ (**18**, tppm* = 6,6′,6″-(methoxymethanetriyl)tris(2-(1H-pyrazol-1-yl)pyridine), and $[Co(hpy)](BPh_4)_2{\cdot}3CH_2Cl_2$ (**19**, hpy = tris(2,2′-bipyrid-6-yl)methanol)[69] share similar coordination cation structures with twist angle φ of 3.80, 2.04, and 19.38°, and deviation parameters of Co^{II} ion coordination geometry towards trigonal prism of 0.589, 0.552, and 2.478, respectively (Fig. 5, twist angle φ defined as the rotation angle of one coordination triangle away from the eclipse conformation to the other, with φ = 60° corresponding to trigonal antiprismatic/octahedral coordination geometry and φ = 0° corresponding to trigonal prism). They all exhibit zero field SMM behavior, with D values of −80.7, −97.2(2), −107.5(4) cm^{-1}, $|E|$ values of 0.6, 9.3(1) × 10^{-3}, 3.5(3) cm^{-1}, and U_{eff} values of 39, 192, 20 cm^{-1}, respectively. Butterfly-like hysteresis loops were observed in **17** and **18**.

3.1.2. CoN_4O_2 Coordination Environment (Mononuclear)

Complex $[Co(L^3)]$ (**20**), constructed using a Schiff-base ligand H_2L^3 (6,6'-((1Z)-((piperazine-1,4-diylbis(propane-3,1-diyl)) bis(azanylylidene))-bis(methanylylidene))bis(2-methoxyphenol)), features top and bottom coordination planes formed by two N and one O atoms, tilting with each other by 6° and twisting by 3° (Fig. 6).[70] Axial anisotropy was revealed with D = −31 cm^{-1}, E = 0.0004 cm^{-1} (determined from magnetization fitting), and D = −41 cm^{-1}, $|E/D|$ = 0.006 (obtained from spin Hamiltonian analysis). Frequency-dependent ac magnetic susceptibility measurements under an applied magnetic field of 1200 Oe yielded U_{eff} = 56.65 cm^{-1}. Moreover, the orientation of the magnetic axes for the first two Kramers doublets was revealed to be dependent on the degree of distortion from prismatic coordination. The smaller the deviation towards idealized D_{3h}, the more axial the g-tensor for the second Kramers doublet.[45]

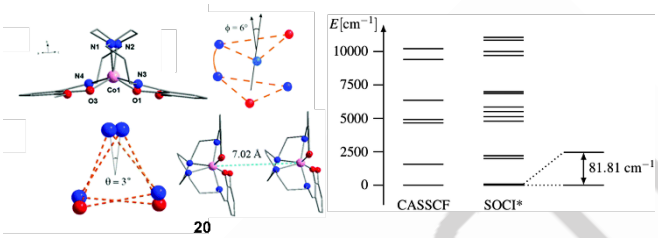

Figure 6. Molecular structure and coordination geometry of complex **20** (left) and its lowest electronic states obtained from *ab initio* calculations (right). Reproduced with permission from Ref. [70].

3.1.3. CoO_6 Coordination Environment (Multinuclear)

In 2013, Gao, *et al.* reported the star-shaped $Co^{II}Co^{III}_3$ complex $(HNEt_3)(Co^{II}Co^{III}_3L^4_6)$ (**21**, H_2L^4 = *R*-4-bromo-2-((2-hydroxy-1-phenylethylimino)methyl)phenol), where the four $Co^{II/III}$ ions form a nearly centered equilateral triangle and the central paramagnetic Co^{II} ion coordinates to six O atoms forming a slightly distorted triangular prism with a deviation of 0.045 (Fig. 7).[71] D = −115 cm^{-1} and E = 2.8 cm^{-1} were obtained from dc magnetization data fitting. It exhibits zero-field slow magnetic relaxation with U_{eff} of 75.76 cm^{-1}. The diamagnetic Co^{III} ions on the periphery were deemed to reduce QTM by weakening the exchange and dipolar interactions. Other $Co^{II}Co^{III}_3$ analogues were synthesized by modifying the substituents of the Schiff-base ligand and changing the counter cations, indicating that the larger the deviation from ideal D_{3h} symmetry, the greater the contribution of transverse anisotropy and the smaller the U_{eff}.[72]

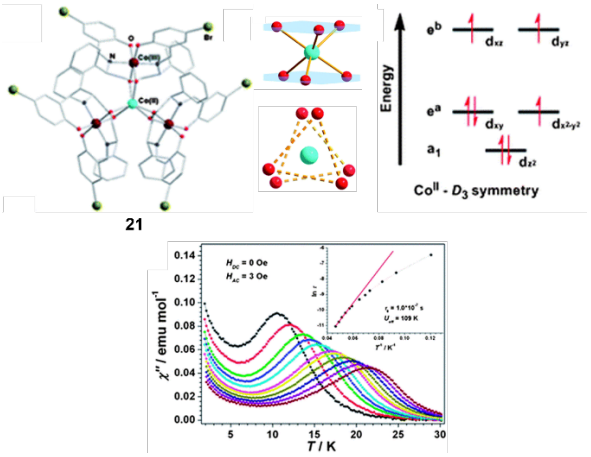

Figure 7. Anionic structure of complex **21**, coordination model of Co^{II} ion, and simplified d^7 electron configuration for the Co^{II} ion with D_3 symmetry (upper); temperature dependence of χ'' at zero dc field of complex **21** (down). Reproduced with permission from Ref. [71].

3.1.4. CoN_4X_2 Coordination Environment (Mononuclear)

Complexes $[CoL^5Cl_2]\cdot H_2O$ (**22**) and $[CoL^5(NCS)_2]\cdot DMSO$ (**23**, L^5 is the bis-condensation product of diacetyl and 2-hydrazinyl-4,6-dimethylpyrimidine) are constructed with a tetradentate ligand L^5 on the equatorial plane and two Cl^-/NCS^- ions on the axis, resulting in coordination geometries deviating from trigonal prism by 5.406 and 6.156, respectively.[73,74] Analysis of dc magnetic data reveals stronger uniaxial magnetic anisotropy for **23**. In the case of **22**, two relaxation processes were observed when the applied magnetic field increased from 1000 to 3200 Oe. The high-frequency relaxation is identified as a combination of the direct one-phonon and two-phonon Raman processes. On the other hand, for **23**, slow magnetic relaxation with U_{eff} of 24.7 cm^{-1} was observed at an applied dc field of 1000 Oe. The different relaxation behavior was largely attributed to considerable impact of the molecular packing in the crystalline structure.

The above reports demonstrate that trigonal prismatic Co^{II} complexes exhibit show slow magnetic relaxation in small or, in many cases, zero external dc fields. The experimental results align with theoretical calculations performed on $Co^{II}N_xO_{6-x}$ (x = 6–0) and $[Co(NH_3)_6]^{2+}$ model complexes with a progressive distortion from the trigonal prismatic coordination geometry. These calculations suggest that when the coordination geometry approaches the end of trigonal prism, the model complexes exhibit the largest and negative *D* value.[67,70]

3.2. Trigonal Antiprismatic Coordination Geometry

Trigonal antiprismatic Co^{II} SMMs are scarce and typically constructed using two tripodal ligands with the two triangular planes inter-distorted. These complexes often exhibit negative *D* value and only show slow magnetic relaxation under external dc fields.

3.2.1. CoN_6 Coordination Environment (Mononuclear)

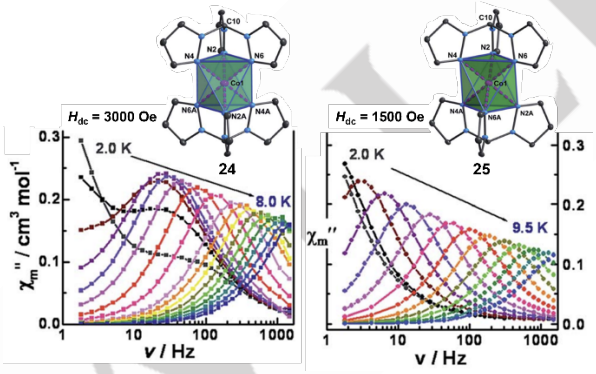

Figure 8. Cationic structures of complexes **24** (left) and **25** (right) and their frequency dependence of χ'' at corresponding dc field. Reproduced with permission from Ref. [75].

In 2016, Zhang, *et al.* reported complexes $[Co(Tpm)_2](ClO_4)_2$ (**24**) and $[Co(Tpm)_2](BPh_4)_2\cdot 2MeCN$ (**25**, Tpm = tris(pyrazol-1-yl)methane), wherein the Co^{II} ions adopt an elongated trigonal antiprismatic coordination geometry with $D = -92$ cm^{-1}, $E = 10.5$ cm^{-1}, and $D = -93$ cm^{-1}, $E = 11.5$ cm^{-1}, respectively (Fig. 8).[75] Under different external dc field, the U_{eff} values range from 30.6(7) to 33.6(5) cm^{-1} for **24**, and 42.5(6) to 44.7(6) cm^{-1} for **25**, significantly deviating from the theoretical energy barriers (232.8 and 236.3 cm^{-1}), indicating a dominance of Raman process. These are the first examples of trigonal antiprismatic Co^{II} complexes displaying filed-induced SMM behavior, suggesting that large uniaxial anisotropy can be achieved in trigonal antiprismatic Co^{II} complexes. Subsequently, complexes $(Tp)_2Co$-1 (**26**), $(Tp)_2Co$-2 (**27**), $Tp_2Co\cdot 2[(CH_3)_2NCS_2]_3Co$ (**28**, Tp = hydridotris(pyrazole) borate), and $(pzTpMe)_2Co$ (**29**, TpMe = tetra(3-methylpyrarole) borate) featuring an elongated trigonal ligand field and twist angle φ of 56.77, 59.40, 59.34, and 58.66°, respectively, were found to exhibit field-induced slow magnetic relaxation with $U_{eff} = 41.9$ cm^{-1} (800 Oe), 10.4 cm^{-1} (800 Oe), 22.6 cm^{-1} (800 Oe), and 20.6 cm^{-1} (1000 Oe), respectively.[76]

3.2.2. CoO_6 Coordination Environment (Multinuclear)

In $[Co_3(Himn)_6]X_2\cdot 2CH_3OH$ (X = Cl, **30**; Br, **31**; I, **32**; and NO_3, **33**, $Himn^-$ = 2-(2-imidazolinyl)phenolate), the central Co^{II} ion is coordinated by six equivalent phenolate-O atoms from a pair of tris-chelate Co^{III} metallo-ligands (Fig. 9).[77] *D* values were determined in the range of −107.3 to −119.7 cm^{-1}. Field-induced SMM behaviors were observed with dominant Raman process.

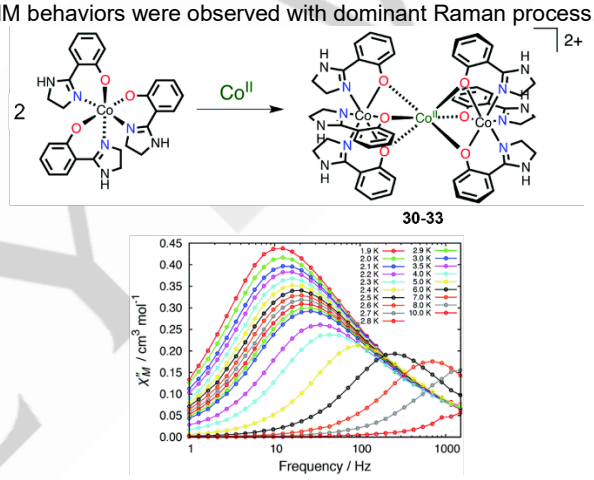

Figure 9. Synthetic procedure of complexes **30-33** (upper) and the frequency dependence of χ'' of complex **30** under 1400 Oe dc field (down). Reproduced with permission from Ref. [77].

Co^{II} SMMs with trigonal antiprism geometry exhibit similar orbital splitting as trigonal prism. There is a certain correlation between the twist angle φ and the SMM performance. When φ is smaller, the magnetic anisotropy is stronger. The reports show that complexes exhibiting zero-field SMM behavior have a φ smaller than 23.5°, whereas complexes show field-induced relaxation behavior when φ values are close to 60°.[76] That is because the local symmetry of Co^{II} ion strongly influences the magnetic anisotropy and SMM behavior. When $\varphi = 0$, the Co^{II} ion is in an ideal trigonal prismatic coordination geometry. Calculations indicate that in this case g_x and g_y are close to 0 and g_z has a large value. That is to say, the complex has a strong axiality and QTM can be suppressed effectively without a dc field. As the increase of φ, the deviation from ideal trigonal prism can change the electron structure of Co^{II} ion and cause the contribution of transverse ZFS, which may influence the component of the ground and excited states wave function, accelerate QTM rate, decrease the effective anisotropy energy barrier. [67,70,76]

3.3. Octahedral Coordination Geometry

The majority of six-coordinated Co^{II} SMMs exhibit quasi-octahedral coordination geometry, primarily due to the easy accessibility through ligand design and synthesis. Unlike trigonal prismatic and trigonal antiprismatic Co^{II} SMMs, which consistently display negative *D* values, octahedral Co^{II} SMMs present both positive and negative values in different coordination environment. A novel mechanism, transverse anisotropy energy barrier for rotation within the *xy* plane, has been proposed to elucidate the slow relaxation of magnetization observed in systems with easy-plane anisotropy.[55] Moreover, a multitude of coordination polymers (1D, 2D, and 3D) featuring Co^{II} ion with octahedral coordination geometry at the nodes have been identified to exhibit slow magnetic relaxation. This discovery has significantly expanded the scope of research on Co^{II}-SMMs. As of now, the reported octahedral Co^{II} SMMs are primarily field-induced, with certain diamagnetic diluted complexes showing zero-field SMM behavior.

3.3.1. CoN_6 Coordination Environment (Mononuclear)

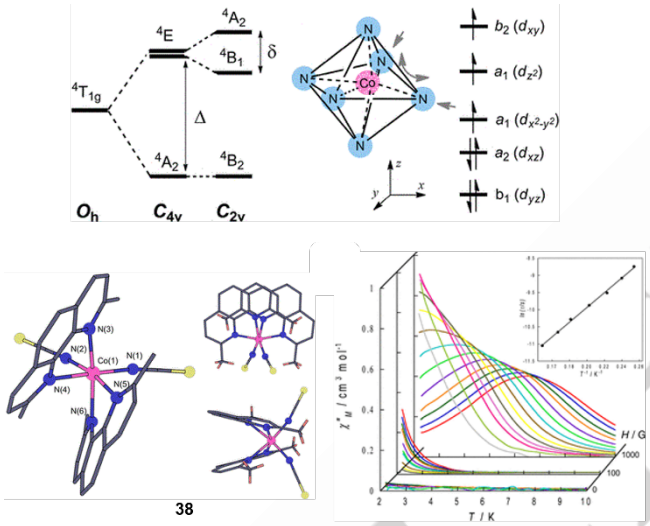

Figure 10. Upper: Simplified energy level diagram for the splitting of the $^4T_{1g}$ ground state in the presence of an external magnetic field parallel to the easy axis and splitting of the *d*-type metal orbitals of an ideal octahedral high-spin Co^{II} Ion after the application of a rhombic (C_{2v}) distortion. Down: molecular structure of complex **38** (left) and its temperature dependence of χ'' under 0, 100, and 1000 Oe dc fields (right). Reproduced with permission from Ref. [55].

In fact, the earliest documentation of octahedral Co^{II} SMMs dates to 2003. Koga's group reported the SMM behavior in frozen solution of the hetero-spin systems, $Co(SCN)_2{\cdot}L^6{}_4$ (**34**, L^6 = 4-(α-diazobenzyl)pyridine) after photo irradiation, and $[CoX_2(4NOpy)_4]$ (X = NCO, **35**; NCS, **36**; and Br, **37**).[78-80] These systems feature Co^{II} ions with octahedral symmetry in their molecular structures. In 2012, Vallejo, *et al*. reported field-induced SMM behavior in *cis*-$[Co^{II}(dmphen)_2(NCS)_2]{\cdot}0.25EtOH$ (**38**, dmphen = 2,9-dimethyl-1,10-phenanthroline, Fig. 10).[55] The octahedral coordination environment in this complex exhibits a rhombic (C_{2v}) distortion with D = +98 cm^{-1}, E = +8.4 cm^{-1}. Under application of a 1000 Oe dc field, frequency-dependent maxima in ac magnetic susceptibility are observed below 10 K, with E_a ranging from 16.2 to 18.1 cm^{-1}. Dc magnetization measurements conducted on single crystals reveal hysteresis loops at temperatures between 0.03 and 1.3 K, with rapid QTM observed at zero dc field. Traditionally, a positive *D* value is counterintuitive to slow magnetic relaxation. However, to explain the SMM behavior exhibited by molecules with positive magnetic anisotropy, transverse anisotropy energy barrier for rotation in the *xy* plane governed by *E* parameter ($E_a = 2E \approx 16.8$ cm^{-1}), rather than the typical axial ones governed by *D* parameter was put forward.[55] It represents a new design strategy to establish a new category of SMMs.

Subsequently, a variety of octahedral Co^{II} SMMs have been reported, For instance, *cis*-$[Co(fpo)_2(NCS)_2]$ (**39**, fpo = 2-(furan-2-yl)-5-(pyridin-2-yl)-1,3,4-oxadiazole) displays a *D* value of –68.6 cm^{-1} with an E/D>0.2.[81] This complex exhibits slow relaxation of magnetization under an applied magnetic field of 1000 Oe via Raman process. *Trans*-$[Co(pto)_2(NCS)_2]$ (**40**, pto = 2-(pyridin-2-yl)-5-(thiophen-2-yl)-1,3,4-oxadiazole)[81] and $[Co(abpt)_2(tcm)_2]$ (**41**, abpt = 4-amino-3,5-bis(2-pyridyl)-1,2,4-triazole and tcm = tricyanomethanes anion)[82] feature Co^{II} ion coordinated by two bidentate N ligands in the equatorial plane and two coordination anions in the axial positions (Fig. 11). Magnetic data analysis reveals D = –39.9 cm^{-1} with E/D > 0.2, and D = +48(2) cm^{-1}, E/D = 0.27(2), respectively. Complex **40** shows slow relaxation of magnetization at a 1000 Oe dc field attributed to the combination of the phonon bottleneck and Raman processes with U_{eff} of 36.2(1) K while **41** exhibits field-induced slow relaxation of magnetization with U_{eff} = 59.9 cm^{-1} under a 3000 Oe dc field.

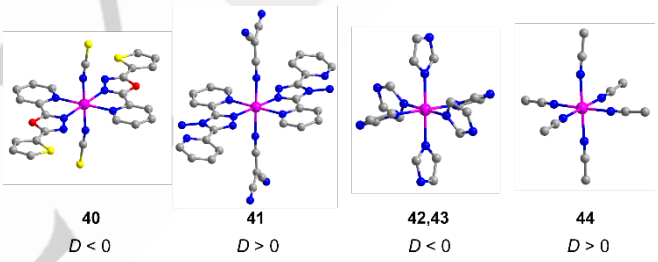

Figure 11. Molecular/cationic structures of complexes **40**, **41**, **42** and **44** and their sign of *D* (from left to right).

Utilizing imidazole as the sole ligand, Co^{II} ions in $[Co(imidazole)_6](BPh_4)_2{\cdot}0.3CH_3CN$ (**42**) and $[Co(imidazole)_6](NO_3)_2$ locate (**43**) adopt quasi-octahedral geometry with minor deviation values of 0.039 and 0.048, respectively (Fig. 11).[83] These complexes exhibit easy-axis anisotropy with parameters B_0^2 = −71.51 cm^{-1}, B_2^2 = 13.03 cm^{-1} for **42**, and B_0^2 = −41.2 cm^{-1}, B_2^2 = 4.22 cm^{-1} for **43** (when there is significant unquenched first order orbital contribution, the zero-field splitting formalism (*D*, *E*) is invalid. Instead, B_0^2 and B_2^2 are used). Furthermore, they show field-induced slow magnetic relaxation with U_{eff} values of 15.0 cm^{-1} and 4.4 cm^{-1}, respectively, at an applied magnetic field of 1000 Oe. However, $[Co(MeCN)_6](BF_4)_2$ (**44**) featuring MeCN as the sole ligand exhibits easy-plane anisotropy with B_2^0= +148.9 cm^{-1}, B_2^2 = ±44.5 cm^{-1} and field-induced slow magnetic relaxation with U_{eff} of 8.6(1) cm^{-1} under a 1500 Oe dc field (Fig. 11).[84]

Employing two tridentate ligands to chelate one Co^{II} ion is a common approach for constructing octahedral Co^{II} complexes. However, due to the strong geometrical constraints imposed by two tridentate ligands, deviations from the ideal octahedron are relatively significant. $[Co^{II}(bppCOOH)_2](ClO_4)_2{\cdot}2Me_2CO$ (**45**, bpp = 2,6-bis-(pyrazol1-yl)pyridine) featuring two *mer*-coordinated bppCOOH ligands clamp the Co^{II} ion in a distorted octahedral

geometry exhibits field-induced slow relaxation of magnetization with a U_{eff} of 11.1 cm^{-1} under a 3000 Oe dc field, and D = 51.6 cm^{-1}, E/D = 0.28 (Fig. 12).[85] Conversely, complex [Co(bpp-COOMe)$_2$](ClO$_4$)$_2$ (**46**) displays easy-axis anisotropy with D = −57.5(7) cm^{-1} and $|E|$ = 15.7(3) cm^{-1} (Fig. 12).[86] Under a 1000 Oe dc field, slow magnetic relaxation is observed with U_{eff}/k_B = 30.3 cm^{-1}. Additionally, the diamagnetic diluted derivative **46** exhibits slow magnetic relaxation in zero field. Modifications to the ligand or composition/structure of the molecule lead to varying degrees of octahedral distortions, consequently influencing magnetization dynamics.[87-91]

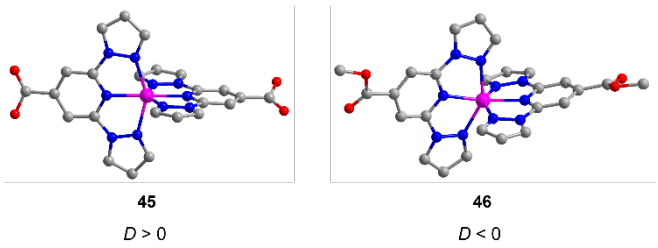

Figure 12. Cationic structures of complexes **45** (left) and **46** (right) and their sign of D.

3.3.2. CoN_xO_{6-x} Coordination Environment (Mononuclear)

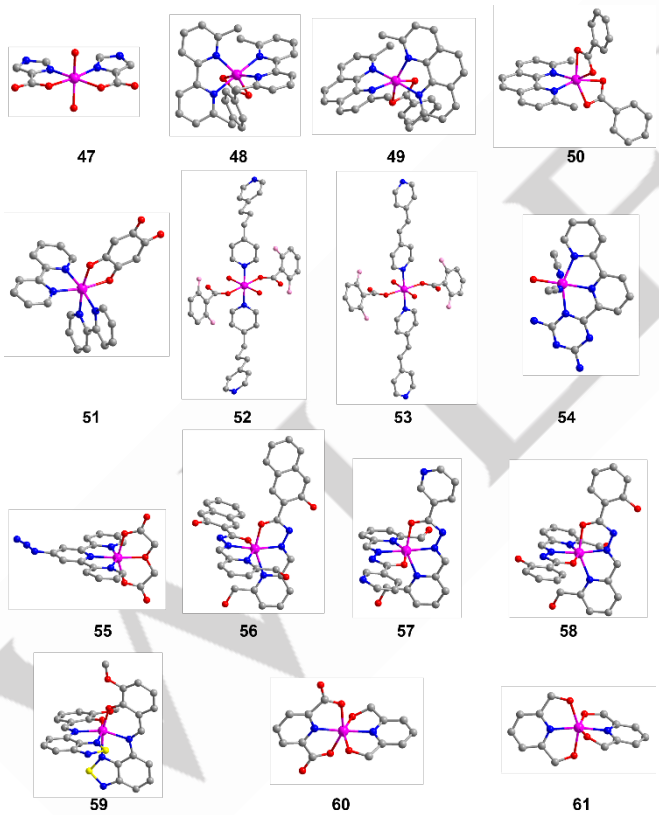

Figure 13. Molecular/cationic structures of complexes **47**-**61**.

Complexes [Co(MCA)$_2$·(H$_2$O)$_2$] (**47**, HMCA = 4-imidazolecarboxylic acid)[92] constructed using two bidentate NO ligands in equatorial plane and two axially coordinated H$_2$O molecules, [Co(dmphen)$_2$(OOCPh)]ClO$_4$·0.5H$_2$O·0.5CH$_3$OH (**48**), [Co(dmbipy)$_2$(OOCPh)]ClO$_4$ (**49**, dmbipy = 6,6′-dimethyl-2,2′-bipyridine, HOOCPh = benzoic acid)[93], [Co(neo)(PhCOO)$_2$] (**50**, neo = neocuproine)[94] and [Co(bpy)$_2$(ClAn)]·EtOH (**51**, bpy = 2,2′-bipyridine, $ClAn^{2-}$ = chloranilate in the *o*-quinone form)[95] constructed using three different bidentate chelate O/N ligands, [Co(L^7)(CH$_3$CN)$_2$(H$_2$O)](ClO$_4$)$_2$·MeCN (**52**, L^7 = 6-(3,5-diamino-2,4,6-triazinyl)2,2′-bipyridine)[89] constructed using one tridentate N ligand and three coordination solvents, and [Co(2,6-dfba)$_2$(bpp′)$_2$(H$_2$O)$_2$]$_n$ (**53**) and [Co(2,6-dfba)$_2$(bpe)$_2$(H$_2$O)$_2$]$_n$ (**54**, 2,6-Hdfba = 2,6-difluorobenzoic acid, bpp′ = 1,3-bis(4-pyridyl)propane, bpe = 1,2-bis(4-pyridyl)ethylene)[96] all exhibit positive D value and field-induced slow relaxation of magnetization (Fig. 13).

Constructed by two tridentate ligands, [Co^{II}(oda)(aterpy)] (**55**, oda^{2-} = oxodiacetate, aterpy = 4-azido-2,2:6,2-terpyridine)[97], [Co(H$_2$L^8)$_2$]·2THF (**56**, H$_3$L^8 = 3-hydroxy-naphthalene-2-carboxylic acid (6-hydroxymethyl-pyridin-2-ylmethylene) hydrazide), [Co(HL^9)$_2$] (**57**, H$_2$L^9 = nicotinic acid (6-hydroxymethyl-pyridin-2-ylmethylene) hydrazide), [Co(H$_2$L^{10})$_2$]·CH$_2$Cl$_2$ (**58**, H$_3$L^{10} = 2-hydroxy-benzoic acid (6-hydroxymethyl-pyridin-2-ylmethylene) hydrazide)[98], [CoL$^{11}_2$]·CH$_2$Cl$_2$ (**59**, HL^{11} = benzothiadiazole-ortho-vanillin)[99], [Co(pydca)(dmpy)]$_2$·H$_2$O (**60**, pydca = pyridine-2,6-dicarboxylato dianion; dmpy = 2,6-dimethanolpyridine)[100], [Co(pydm)$_2$](dnbz)$_2$ (**61**, pydm = 2,6-pyridinedimethanol, dnbz = 3,5-dinitrobenzoato)[101] and [Co(pydm)$_2$](mdnbz)$_2$ (**62**, mdnbz = 3,5-dinitro-4-methylbenzoate)[102] all exhibit negative D values and field-induced SMM behavior with U_{eff} values below 27.7 cm^{-1} (Fig. 13).

3.3.3. CoN_4X_2 Coordination Environment (Mononuclear)

Complex [Co(py)$_4$(SCN)$_2$] (**63**) features axial compressed octahedron and complexes [Co(py)$_4$Cl$_2$]·H$_2$O (**64**) and [Co(py)$_4$Br$_2$] (**65**) feature axial elongated coordination octahedron, displaying D = +46.8(3) cm^{-1}, $|E|$ = 1.42(4) cm^{-1}; D = +68.2(5) cm^{-1}, $|E|$ = 2.74(3) cm^{-1}; and D = +61.5(4) cm^{-1}, $|E|$ = 2.42(2) cm^{-1}, respectively.[103] The different axial ligand fields influence only the magnitude rather than the sign of D. Under 1000 Oe, 1500 Oe, and 500 Oe dc fields, these complexes exhibit slow magnetic relaxations with U_{eff} values of 22.4, 19.4, and 20.4 cm^{-1}, respectively. A magneto-structural correlation performed on complex **64**, changing only the axial and transverse ligand fields while keeping other structural parameters the same indicates that it is possible to attain both axial and easy plane magnetic anisotropy by fine-tuning the ligand fields. Additionally, an axial-to-equatorial bond length ratio of 1.02 or less is expected to result in a more negative D value, while a ratio of 1.06 or greater is expected to result in a more positive D value. In addition, the structurally similar compounds with higher D values have also been reported.[104,105]

3.3.4. CoO_6 Coordination Environment (Mononuclear)

Complex Et$_4$N[Co^{II}(hfac)$_3$] (**66**, hfac = hexafluoroacethyl acetonate), constructed with three bidentate chelate O ligand, adopts an axial compressed octahedron coordination geometry around Co^{II} ion, characterized by D = +117.8 cm^{-1} and E/D = 0.0853.[106] Ac susceptibility measurements under 1000 Oe reveal two sets of frequency-dependent maxima in the temperature range of 1.8-3.3 K with U_{eff} values of 14.3 and 12.5 cm^{-1}, attributed to SIM behavior arising from axial and rhombic

anisotropies, respectively. In complex $(NBu_4)[Co(piv)_3]$ **(67,** piv = pivalate**)**, three pivalate anions coordinate to one Co^{II} ion with deviation values relative to octahedron and trigonal prism of 7.06 and 9.34, respectively, and twist angle φ of 28.7°.[107] The fits of dc magnetic data yield B_2^0 = −134.4 cm^{-1} and B_2^2 = 37.5 cm^{-1}. Ac magnetic susceptibility measurements reveal field-induced slow magnetic relaxation with U_{eff} = 20.7 cm^{-1} (1000 Oe).

To mitigate dipolar-dipolar interaction, which typically accelerates QTM and compromise SMM behavior, Sato, *et. al*. reported the first polyoxometalate (POM)-based mononuclear Co^{II} SMM (**68** where the Co^{II} ion are separated from each other by at least 14 Å due to the presence of bulky ligands.[108] Magnetization data fitting results in D = 95.2 cm^{-1} and E = 7.18 cm^{-1}. Under 1000 Oe, characteristic SMM behavior is observed with U_{eff} = 13.5 cm^{-1}. Sahu, *et al*. employed large non-magnetic POMs as diamagnetic components to separate $[Co(H_2O)_6]^{2+}$ units in $[\{Co(H_2O)_6\}^{2+}\{Na_4V_{10}O_{28}\}^{2-}]$ (**69**), ensuring each $[Co(H_2O)_6]^{2+}$ unit is separated by a minimum distance of 9 Å.[109] Magnetic studies reveal easy-axis anisotropy (D = –102 cm^{-1}) and field induced slow magnetic relaxation behavior with U_{eff} = 34.8 cm^{-1}.

3.3.5. CoN_xO_{6-x} Coordination Environment (Multinuclear)

There are also reports of multinuclear complexes comprising only one high-spin Co^{II} ion alongside other diamagnetic ions, exhibiting slow magnetic relaxation behavior.[110] From a magnetic perspective, these complexes can be considered as mononuclear SMMs. For instance, the Co^{II}–Y^{III} complex $[Co(\mu\text{-}L^{12})(\mu\text{-}OAc)Y(NO_3)_2]$ (**70**, H_2L^{12} = N,N',N''-trimethyl-N,N''-bis(2-hydroxy-3-methoxy-5-methylbenzyl)-diethylenetriamine) features a Co^{II} ion adopting a CoN_3O_3 trigonally distorted octahedral coordination sphere, with the deviation value of 2.8 towards octahedron (Fig. 14).[57] Easy-plane anisotropy was found with D = +41.7 (or 47) cm^{-1}, E = 1.6 (or 2.0) cm^{-1}. It shows field-induced slow magnetic relaxation below 5 K with U_{eff} = 15.7 cm^{-1}. Further analysis of the slow magnetic relaxation suggests a predominant optical acoustic Raman process. Similar complexes with varying bridging carboxylate groups have been reported, all displaying positive D values and field-induced SMM behavior.[111,112]

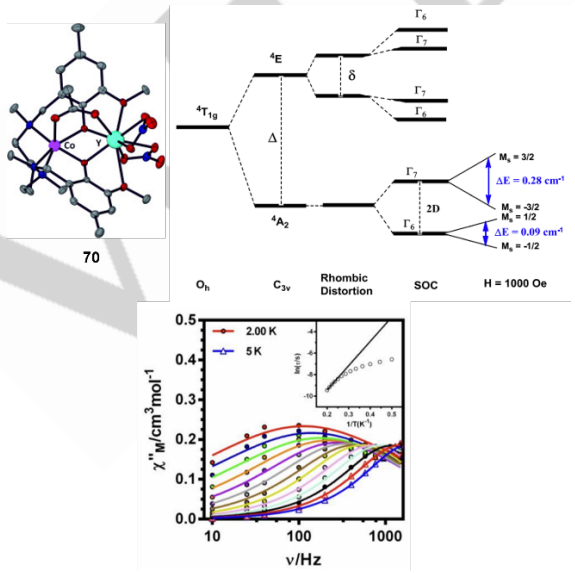

Figure 14. Molecular structure of complex **70** (upper left); qualitative splitting of the $^4T_{1g}$ by axial and rhombic distortions, SOC and an applied magnetic field of 1000 Oe (upper right); and frequency dependence of χ'' of **70** under 1000 Oe dc field (down). Reproduced with permission from Ref. [57].

In complexes $[Co^{III}Co^{II}(L^{13}H_2)_2(X)(H_2O)](H_2O)_m$ (H_4L^{13} = 2-[{(2-hydroxy-3-methoxyphenyl)methylene}amino]-2-(hydroxymethyl)-1,3-propanediol, X = Cl and m = 4, **71**; X = Br and m = 4, **72**; X = NO_3 and m = 3, **73**,) the Co^{II} ion coordination geometries exhibit deviation values from octahedron of 0.74, 1.07, and 1.43, respectively.[113] Analysis of M vs H data yields D = −7.4 cm^{-1} with $|E/D| < 1 \times 10^{-3}$ for **71**, and D = −9.7 cm^{-1} with $|E/D| < 1 \times 10^{-4}$ for **72**. Both complexes display slow relaxation of magnetization under a 1000 Oe dc field with U_{eff} values of 7.9 cm^{-1} and 14.5 cm^{-1}, respectively. Complex **73**, however, does not show any SMM behavior due to comparatively little magnetic anisotropy.

In the trinuclear Co^{III}-Co^{II}-Co^{III} complexes $[(L^{14})_4Co_3(H_2O)_2](NO_3)_4\cdot CH_3OH\cdot 5H_2O$ (**74**, HL^{14} is the condensation product of pyrazine carbohydrozone and 4-imidazocarboxylate) and $[(L^{15})_4Co_3(H_2O)_2](NO_3)_4\cdot 6H_2O$ (**75**, HL^{15} is the condensation product of pyrazine carbohydrozone and pyridine-2-carboxylate), the central Co^{II} ion is coordinated with two sets of NO bidentate units on the equatorial plane from the Co^{III} metallo-ligands and two H_2O molecules on the axial (Fig. 15).[56] The octahedral geometry is axially elongated in **74** while compressed in **75** with greater distortion. Easy-plane anisotropy is observed with D = 18.6 ± 0.27 cm^{-1}, E = −1.7 ± 0.1 cm^{-1} for **74**, and D = 31.9 ± 0.33 cm^{-1}, E = −3.0 ± 0.1 cm^{-1} for **75**. Under applied fields, ac magnetic measurements reveal nearly zero χ'' for **74** and frequency-dependent χ'' maxima below 10 K with E_a = 5.6 cm^{-1} (1000 Oe) for **75**, closed to the transverse energy barrier for rotation in the *x*-*y* plane, $E(S^2 - 1/4)$ = 6.0 cm^{-1}.

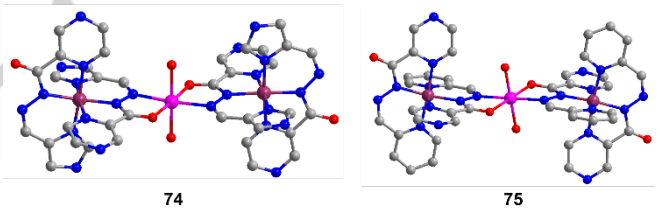

Figure 15. Cationic structures of complexes **74** (left) and **75** (right).

3.3.6. CoN_6 Coordination Environment (Coordination Polymer)

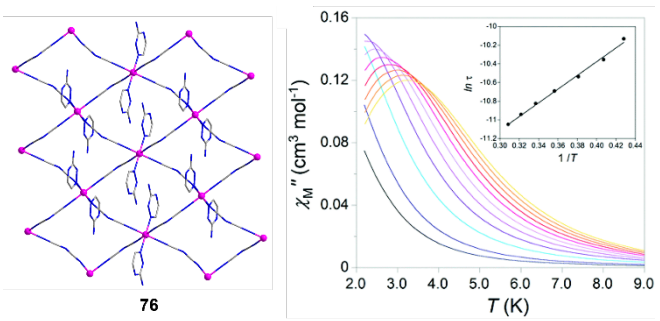

Figure 16. 2D structure of complex **76** (left) and its frequency dependence of χ'' under a 1000 Oe dc field (right). Inset: ln(τ) *vs.* 1/*T*, the solid line represents the Arrhenius plot. Reproduced with permission from Ref. [114].

The 2D coordination polymer $[Co(dca)_2(atz)_2]_n$ (**76**, dca = dicyanamide, atz = 2-amino-1,3,5-triazine) features Co^{II} ions bridged by $\mu_{1,5}$-dca, exhibiting field-induced SIM behavior (Fig. 16).[114] Each Co^{II} ion, positioned at the crystallographic inversion center, coordinates with four nitrile N atoms at equatorial sites and two N atoms of the atz ligand at the axial sites, forming an elongated octahedron. E_a of 5.1 cm^{-1} was obtained under a dc field of 1000 Oe.

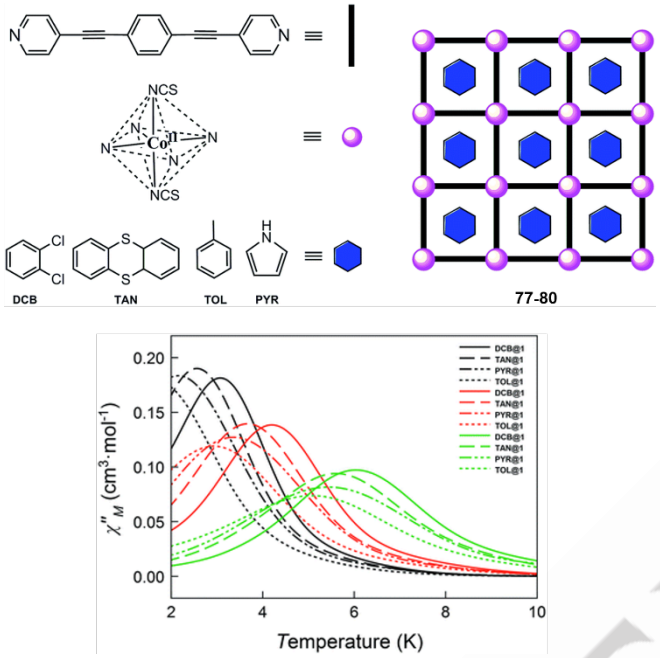

Figure 17. Structural representation of $[Co(bpeb)_2(NCS)_2]\cdot nG$ (upper) and their temperature dependence of χ'' under 1000 Oe dc field at 672 (black), 2043 (orange) and 10 000 Hz (green) frequencies (down). Reproduced with permission from Ref. [115].

In 2016, Vallejo *et al.* reported 2D SIM-MOFs $[Co(bpeb)_2(NCS)_2]\cdot nG$ (**77-80**, bpeb = 1,4-bis(pyridine-4-ylethynyl)benzene), where Co^{II} ions are interconnected by long organic spacers, situated within a distorted octahedral environment characterized by longer equatorial Co–N bonds compared to axial ones (Fig. 17).[115] Through the exchange of guest molecules (G), DCB (**77**), TAN (**78**), TOL (**79**), and PYR (**80**) within the pores, four complexes were obtained, each exhibiting D values of 64.9(9) cm^{-1}, 67.1(9) cm^{-1}, 84.4(4) cm^{-1}, and 70.3(9) cm^{-1} along with rhombic $E/D \approx 0.12$. Ac susceptibilities at 1000 Oe dc field were analyzed by two different Orbach processes with Ea = 31.3 cm^{-1}, 8.8 cm^{-1}; 17.1 cm^{-1}, 6.2 cm^{-1}; 11.5 cm^{-1}, 2.5 cm^{-1}; and 21.0 cm^{-1}, 4.9 cm^{-1} for **77-80**, respectively. The asymmetry in the axial and perpendicular g-factor of Co^{II} ions was proposed to account for the dual relaxations (parallel and transverse). Additionally, other 1D and 2D Co^{II} complexes with axial compressed coordination octahedra and easy-plane anisotropy have been reported, exhibiting field-induced slow magnetic relaxation behavior.[116-118]

3.3.7. CoN_xO_{6-x} Coordination Environment (Coordination Polymer)

2D polymers $[Co(ppad)_2]_n$ (**81**, ppad = N^3-(3-pyridoyl)-3-pyridinecarboxamidrazone)[119] and $\{[Co(bmzbc)_2]\cdot 2DMF\}_n$ (**82**, bmzbc⁻ = 4-(benzimidazole-1-yl)benzoate)[120] were reported to exhibit field-indued SMM behavior, with D = 76 cm^{-1}, E = 6.5 cm^{-1} and D = 60.4 cm^{-1}, E = 8.0 cm^{-1}, respectively. Under 2000 Oe dc field, E_a values of 11.37 cm^{-1} and 8.7 cm^{-1} were obtained, respectively. The 1D complex $[Co(3\text{-}Hppt)_2(adip)(H_2O)_2]\cdot 2H_2O$ (**83**, 3-Hppt = 3-phenyl-5-(pyridin-3-yl)-1,2,4-triazole, adip = adipic acid)[121] and 3D framework $[Co(1,4\text{-}bib)_{1.5}(5\text{-}hip)(H_2O)]_n$ (**84**, 1,4-bib = 1,4-bis(1-imidazolyl)benzene, 5-hip = 5-hydroxyisophthalic acid)[122] were found to exhibit easy axial magnetic anisotropy, with D = –33.9 cm^{-1}, $|E|$ = 6.4 cm^{-1}, and D = –102 cm^{-1}, E = 0.36 cm^{-1}, respectively. They display field-induced dual magnetic relaxation processes with U_{eff} of 20.16 cm^{-1} (1200 Oe) and U_{eff} = 12.8 cm^{-1} (1000 Oe).

For Co^{II} SMMs demonstrating easy-plane magnetic anisotropy, another explanation for the mechanism of slow magnetic relaxation has been discussed in Co^{II} SMMs with other coordination numbers.[32,123,124] In addition to the relaxation stemming from the transverse anisotropy barrier due to a significant E value, there is the field-induced phonon bottleneck effect, where direct relaxation becomes so slow that an Orbach relaxation pathway occurs through the excited M_S = ±3/2 levels. However, in many cases, neither mechanism is applicable, and magnetic relaxation is often attributed to a Raman process. Further study of these mechanisms is warranted.

4. Summary and Outlook

Based on the aforementioned finding, Co^{II} SMMs with a trigonal prismatic coordination environment often exhibit significant uniaxial magnetic anisotropy and slow relaxation of magnetization under zero external dc field while Co^{II} SMMs with trigonal antiprismatic configuration also demonstrate large easy-axis anisotropy, but external dc field is required to induce slow magnetic relaxation. Octahedral Co^{II} SMMs, constituting the majority and showcasing the most diverse structures, display both easy-axis or easy-plane anisotropy in different cases. External dc field is also indispensable to initiate slow magnetic relaxation. Literature indicates that the Co^{II} SMMs showing zero-field slow magnetic relaxation behavior typically feature a φ smaller than 23.5°. In addition, challenges persist. Many Co^{II} SMMs with strong magnetic anisotropy and high first excitation energy yield only minimal U_{eff} values without hysteresis loop regardless of molecular structure. This could be attributed to prevalent under barrier relaxation processes with Raman process being more efficient at high temperatures due to the deficiency of high-energy phonons, which pose a significant obstacle to further SMMs development. Hence, rather than solely focusing on D, U_{eff}, and T_B values, a holistic approach, considering magnetic anisotropy and how the spin interact with crystal lattice is necessary to gain insight into controlling the contributions of different relaxation processes. Achieving this requires collaborative effort among synthetic chemists, theoretical physicists and experimental spectroscopists. Moreover, there is a lack of solid explanation and experimental characterization regarding the magnetic anisotropy and slow relaxation mechanism of certain Co^{II}-SMMs with positive D value. Extra cautious and rigor should be taken when interpreting results and characterizations, such as the field-induced slow magnetic relaxation behavior given the multifaceted and complex influence of external filed beyond merely suppressing QTM. Additionally, exploring SMM systems based on

4*d* and 5*d* metal ions should not be overlooked due to their large spin-orbit coupling, which may lead to advanced SMM properties in the near future.

Acknowledgements

We thank the Fonds de la Recherche Scientifique-FNRS (PDR T.0095.21, FC 53249), National Natural Science Foundation of China (No. 22121005) and the Ministry of Education of China (grant ref: B12015).

Keywords: six-coordinated Co complex • single-molecule magnet • slow magnetic relaxation • magnetic anisotropy • zero-filed splitting

[1] R. Sessoli, H. L. Tsai, A. R. Schake, S. Wang, J. B. Vincent, K. Folting, D. Gatteschi, G. Christou, D. N. Hendrickson, *J. Am. Chem. Soc*. **1993**, *115*, 1804.

[2] D. Gatteschi, R. Sessoli, J. Villain, *Molecular Nanomagnets*, Oxford University Press: Oxford, **2007**.

[3] A. Zabala-Lekuona, J. M. Seco, E. Colacio, *Coord. Chem. Rev*. **2021**, *441*, 213984.

[4] A. J. Tasiopoulos, A. Vinslava, W. Wernsdorfer, K. A. Abboud, G. Christou, *Angew. Chem. Int. Ed.* **2004**, *116*, 2169.

[5] A. M. Ako, I. J. Hewitt, V. Mereacre, R. Clérac, W. Wernsdorfer, C. E. Anson, A. K. Powell, *Angew. Chem. Int. Ed.* **2006**, *45*, 4926.

[6] E. Ruiz, J. Cirera, J. Cano, S. Alvarez, C. Loose, J. Kortus, *Chem. Commun*. **2008**, *1*, 52.

[7] N. Ishikawa, M. Sugita, T. Ishikawa, S. Y. Koshihara, Y. Kaizu, *J. Am. Chem. Soc*. **2003**, *125*, 8694.

[8] Y. S. Meng, S. D. Jiang, B. W. Wang, S. Gao, *Acc. Chem. Res*. **2016**, *49*, 2381.

[9] M. Feng, M. L. Tong, *Chem. Eur. J*. **2018**, *24*, 7574.

[10] J. Liu, Y. C. Chen, J. L. Liu, V. Vieru, L. Ungur, J. H. Jia, L. F. Chibotaru, Y. Lan, W. Wernsdorfer, S. Gao, X. M. Chen, *J. Am. Chem. Soc*. **2016**, *138*, 5441.

[11] M. Wang, Y. Guo, Z. Han, X. Cheng, Y. Q. Zhang, W. Shi, P. Cheng, *Inorg. Chem*. **2022**, *61*, 9785.

[12] S. D. Jiang, B. W. Wang, H. L. Sun, Z. M. Wang, S. Gao, *J. Am. Chem. Soc*. **2011**, *133*, 4730.

[13] K. Jia, X. Meng, M. Wang, X. Gou, Y. X. Wang, N. Xu, W. Shi, P. Cheng, *Chem. Commun*. **2021**, *57*, 3607.

[14] F. S. Guo, B. M. Day, Y. C. Chen, M. L. Tong, A. Mansikkamäki, R. A. Layfield, *Science* **2018**, *362*, 1400.

[15] C. A. Gould, K. R. McClain, D. Reta, J. G. Kragskow, D. A. Marchiori, E. Lachman, E. S. Choi, J. G. Analytis, R. D. Britt, N. F. Chilton, B. G. Harvey, J. R. Long, *Science* **2022**, *375*, 198.

[16] P. Cheng, Lanthanides : Fundamentals and Applications. Elsevier, 2023.

[17] J. M. Zadrozny, D. J. Xiao, M. Atanasov, G. J. Long, F. Grandjean, F. Neese, J. R. Long, *Nat. Chem*. **2013**, *5*, 577.

[18] A. K. Bar, C. Pichon, J. P. Sutter, *Coord. Chem. Rev*. **2016**, *308*, 346.

[19] G. Bhatt, T. Sharma, S. K. Gupta, F. Meyer, G. Rajaraman, R. Murugavel, *Inorg. Chem*. **2023**, *62*, 18915.

[20] P. K. Sahu, R. Kharel, S. Shome, S. Goswami, S. Konar, *Coord. Chem. Rev*. **2023**, *475*, 214871.

[21] S. Tripathi, S. Vaidya, K. U. Ansari, N. Ahmed, E. Riviere, L. Spillecke, C. Koo, R. Klingeler, T. Mallah, G. Rajaraman, M. Shanmugam, *Inorg. Chem*. **2019**, *58*, 9085.

[22] A. Sarkar, S. Dey, G. Rajaraman, *Chem. Eur. J*. **2020**, *26*, 14036.

[23] P. Comba, G. Rajaraman, A. Sarkar, G. Velmurugan, *Dalton Trans*. **2022**, *51*, 5175.

[24] Y. Rechkemmer, F. D. Breitgoff, M. Van Der Meer, M. Atanasov, M. Hakl, M. Orlita, P. Neugebauer, F. Neese, B. Sarkar, J. Van Slageren, *Nat. Commun*. **2016**, *7*, 10467.

[25] S. Vaidya, S. Tewary, S. K. Singh, S. K. Langley, K. S. Murray, Y. Lan, W. Wernsdorfer, G. Rajaraman, M. Shanmugam, *Inorg. Chem*. **2016**, *55*, 9564.

[26] X. Liu, X. Feng, K. R. Meihaus, X. Meng, Y. Zhang, L. Li, J. L. Liu, K. S. Pedersen, L. Keller, W. Shi, Y. Q. Zhang, P. Cheng, J. R. Long, *Angew. Chem. Int. Ed*. **2020**, *59*, 10610.

[27] Y. S. Meng, Z. Mo, B. W. Wang, Y. Q. Zhang, L. Deng, S. Gao, *Chem. Sci*. **2015**, *6*, 7156.

[28] M. Wang, X. Gou, W. Shi, P. Cheng, *Chem. Commun*. **2019**, *55*, 11000.

[29] X. Ma, Z. Zhang, W. Shi, L. Li, J. Zou, P. Cheng, *Chem. Commun.* **2014**, *50*, 6340.

[30] X. N. Yao, J. Z. Du, Y. Q. Zhang, X. B. Leng, M. W. Yang, S. D. Jiang, Z. X. Wang, Z. W. Ouyang, L. Deng, B. W. Wang, S. Gao, *J. Am. Chem. Soc.* **2017**, *139*, 373.

[31] P. C. Bunting, M. Atanasov, E. Damgaard-Møller, M. Perfetti, I. Crassee, M. Orlita, J. Overgaard, J. Slageren, F. Neese, J. R. Long, *Science* **2018**, *362*, 1378.

[32] A. Lunghi, F. Totti, R. Sessoli, S. Sanvito, *Nat. Commun*. **2017**, *8*, 14620.

[33] Y. Q. Zhai, Y. Z. Zheng, *J. Mater. Chem. C* **2021**, *9*, 8096.

[34] J. Long, A. O. Tolpygin, E. Mamontova, K. A. Lyssenko, D. Liu, M. D. Albaqami, L. F. Chibotaru, Y. Guari, J. Larionova, A. A. Trifonov, *Inorg. Chem. Front*. **2021**, *8*, 1166.

[35] S. Gómez-Coca, A. Urtizberea, E. Cremades, P. J. Alonso, A. Camón, E. Ruiz, F. Luis, *Nat. Commun*. **2014**, *5*, 4300.

[36] J. Juráková, I. Šalitroš, *Monatsh. Chem.* **2022**, *153*, 1001.

[37] C. Benelli, D. Gatteschi, *Introduction to molecular magnetism: from transition metals to lanthanides*, John Wiley & Sons. **2015**.

[38] R. Boča, *Coord. Chem. Rev*. **2004**, *248*, 757.

[39] J. R. Gispert, *Coordination Chemistry*, Wiley-VCH, Weinheim, **2008**.

[40] G. A. Craig, M. Murrie, *Chem. Soc. Rev*. **2015**, *44*, 2135.

[41] G. Aromí, E. K. Brechin, *Struct. Bonding* **2006**, *122*, 1-67.

[42] O. Waldmann, *Inorg. Chem*. **2007**, *46*, 10035.

[43] N. F. Chilton, R. P. Anderson, L. D. Turner, A. Soncini, K. S. Murray, *J. Comput. Chem*. **2013**, *34*, 1164.

[44] F. Lloret, M. Julve, J. Cano, R. Ruiz-García, E. Pardo, *Inorg. Chim. Acta*, **2008**, *361*, 3432.

[45] B. N. Figgis, M. A. Hitchman, *Ligand field theory and its applications*, *1st ed*, Wiley-VCH: New York, **2000**.

[46] A. Abragam, B. Bleaney, *Electron paramagnetic resonance of transition ions*, Clarendon Press, Oxford, **1970**.

[47] A. Furrer, J. F. Mesot, T, Strässle, *Neutron scattering in condensed matter physics*, World Scientific Publishing Company, **2009**.

[48] B. Henderson, G. F. Imbusch, *Optical spectroscopy of inorganic solids*, Oxford University Press, **2006**.

[49] N. Kaltsoyannis, J. E. McGrady, *Principles and applications of density functional theory in inorganic chemistry*, Springer Science & Business Media, **2004**.

[50] A. Szabo, N. S. Ostlund, *Modern quantum chemistry: introduction to advanced electronic structure theory*, Courier Corporation. **2012**.

[51] C. E. Jackson, I. P. Moseley, R. Martinez, S. Sung, J. M. Zadrozny, *Chem. Soc. Rev.* **2021**, *50*, 6684.

[52] J. L. Liu, Y. C. Chen, M. L. Tong, *Chem. Soc. Rev*. **2018**, *47*, 2431.

[53] J. M. Zadrozny, M. Atanasov, A. M. Bryan, C. Y. Lin, B. D. Rekken, P. P. Power, F. Neese, J. R. Long, *Chem. Sci*. **2013**, *4*, 125.

[54] A. Swain, T. Sharma, G. Rajaraman, *Chem. Commun*. **2023**, *59*, 3206.

[55] J. Vallejo, I. Castro, R. Ruiz-García, J. Cano, M. Julve, F. Lloret, G. D. Munno, W. Wernsdorfer, E. Pardo, *J. Am. Chem. Soc.* **2012**, *134*, 15704.

[56] D. Wu, X. Zhang, P. Huang, W. Huang, M. Ruan, Z. W. Ouyang, *Inorg. Chem*. **2013**, *52*, 10976.

[57] E. Colacio, J. Ruiz, E. Ruiz, E. Cremades, J. Krzystek, S. Carretta, J. Cano, T. Guidi, W. Wernsdorfer, E. K. Brechin, *Angew. Chem. Int. Ed*. **2013**, *52*, 9130.

[58] S. Gomez-Coca, E. Cremades, N. Aliaga-Alcalde, E. Ruiz, *J. Am. Chem. Soc.* **2013**, *135*, 7010.

[59] V. Chandrasekhar, R. Azhakar, B. M. Pandian, R. Boomishankar, A. Steiner, *Dalton Trans.* **2008**, *43*, 5962.

[60] O. A. Varzatskii, L. V. Penkova, S. V. Kats, A. V. Dolganov, A. V. Vologzhanina, A. A. Pavlov, V. V. Novikov, A. S. Bogomyakov, V. N. Nemykin, Y. Z. Voloshin, *Inorg. Chem*. **2014**, *53*, 3062.

[61] V. V. Novikov, A. A. Pavlov, Y. V. Nelyubina, M. E. Boulon, O. A. Varzatskii, Y. Z. Voloshin, R. E. P. Winpenny, *J. Am. Chem. Soc.* **2015**, *137*, 9792.

[62] A. A. Pavlov, S. A. Savkina, A. S. Belov, Y. V. Nelyubina, N. N. Efimov, Y. Z. Voloshin, V. V. Novikov, *Inorg. Chem.* **2017**, *56*, 6943.

[63] A. A. Pavlov, D. Y. Aleshin, S. A. Savkina, A. S. Belov, N. N. Efimov, J. Nehrkorn, M. Ozerov, Y. Z. Voloshin, Y. V. Nelyubina, V. V. Novikov, *ChemPhysChem* **2019**, *20*, 1001.

[64] A. A. Pavlov, Y. V. Nelyubina, S. V. Kats, L. V. Penkova, N. N. Efimov, A. O. Dmitrienko, A. V. Vologzhanina, A. S. Belov, Y. Z. Voloshin, V. V. Novikov, *J. Phys. Chem. Lett.* **2016**, *7*, 4111.

[65] A. Landart-Gereka, M. M. Quesada-Moreno, I. F. Díaz-Ortega, H. Nojiri, M. Ozerov, J. Krzystek, M. A. Palacios, E. Colacio, *Inorg. Chem. Front.* **2022**, *9*, 2810.

[66] M. Wang, Z. Han, X. Gou, W. Shi, Y. Q. Zhang, P. Cheng, *Chem. Eur. J.* **2023**, *29*, e202301693.

[67] T. J. Ozumerzifon, I. Bhowmick, W. C. Spaller, A. K. Rappé, M. P. Shores, *Chem. Commun.* **2017**, *53*, 4211.

[68] B. Yao, Y. F. Deng, T. Li, J. Xiong, B. W. Wang, Z. Zheng, Y. Z. Zhang, *Inorg. Chem.* **2018**, *57*, 14047.

[69] B. Yao, M. K. Singh, Y. F. Deng, Y. N. Wang, K. R. Dunbar, Y. Z. Zhang, *Inorg. Chem.* **2020**, *59*, 8505.

[70] Y. Peng, T. Bodenstein, K. Fink, V. Mereacre, C. E. Anson, A. K. Powell, *Phys. Chem. Chem. Phys.* **2016**, *18*, 30135.

[71] Y. Y. Zhu, C. Cui, Y. Q. Zhang, J. H. Jia, X. Guo, C. Gao, K. Qian, S. D. Jiang, B. W. Wang, Z. M. Wang, S. Gao, *Chem. Sci.* **2013**, *4*, 1802.

[72] Y. Y. Zhu, Y. Q. Zhang, T. T. Yin, C. Gao, B. W. Wang, S. Gao, *Inorg. Chem.* **2015**, *54*, 5475.

[73] Y. P. Tupolova, I. N. Shcherbakov, L. D. Popov, V. E. Lebedev, V. V. Tkachev, K. V. Zakharov, A. N. Vasiliev, D. V. Korchagin, A. V. Palii, S. M. Aldoshin, *Dalton Trans.* **2019**, *48*, 6960.

[74] Y. P. Tupolova, I. N. Shcherbakov, D. V. Korchagin, V. V. Tkachev, V. E. Lebedev, L. D. Popov, K. V. Zakharov, A. N. Vasiliev, A. V. Palii, S. M. Aldoshin, *J. Phys. Chem. C* **2020**, *124*, 25957.

[75] Y. Z. Zhang, S. Gómez-Coca, A. J. Brown, M. R. Saber, X. Zhang, K. R. Dunbar, *Chem. Sci.* **2016**, *7*, 6519.

[76] J. Zhang, J. Li, L. Yang, C. Yuan, Y. Q. Zhang, Y. Song, *Inorg. Chem.* **2018**, *57*, 3903.

[77] R. Mitsuhashi, K. S. Pedersen, T. Ueda, T. Suzuki, J. Bendix, M. Mikuriya, *Chem. Commun.* **2018**, *54*, 8869.

[78] S. Karasawa, G. Zhou, H. Morikawa, N. Koga, *J. Am. Chem. Soc.* **2003**, *125*, 13676.

[79] S. Kanegawa, S. Karasawa, M. Nakano, N. Koga, *Chem. Commun.* **2004**, *15*, 1750.

[80] S. Kanegawa, S. Karasawa, M. Nakano, N. Koga, *Bull. Chem. Soc. Jpn.* **2006**, *79*, 1372.

[81] P. Zoufalý, A. Kliuikov, E. Čižmár, I. Císařová, R. Herchel, *Eur. J. Inorg. Chem.* **2021**, *12*, 1190.

[82] R. Herchel, L. Váhovská, I. Potočňák, Z. Trávníček, *Inorg. Chem.* **2014**, *53*, 5896.

[83] L. Chen, J. Zhou, H. H. Cui, A. H. Yuan, Z. Wang, Y. Q. Zhang, Z. W. Ouyang, Y. Song, *Dalton Trans.* **2018**, *47*, 2506.

[84] M. R. Saber, M. K. Singh, K. R. Dunbar, *Chem. Commun.* **2020**, *56*, 8492.

[85] V. García-López, F. J. Orts-Mula, M. Palacios-Corella, J. M. Clemente-Juan, M. Clemente-León, E. Coronado, *Polyhedron* **2018**, *150*, 54.

[86] L. Rigamonti, N. Bridonneau, G. Poneti, L. Tesi, L. Sorace, D. Pinkowicz, J. Jover, E. Ruiz, R. Sessoli, A. Cornia, *Chem. Eur. J.* **2018**, *24*, 8857.

[87] F. Kobayashi, R. Ohtani, M. Nakamura, L. F. Lindoy, S. Hayami, *Inorg. Chem.* **2019**, *58*, 7409.

[88] B. Brachňaková, S. Matejová, J. Moncol, R. Herchel, J. Pavlik, E. Moreno-Pineda, M. Ruben, I. Šalitroš, *Dalton Trans.* **2020**, *49*, 1249.

[89] M. Palacios-Corella, V. García-López, C. Sánchez-Sánchez, J. M. Clemente-Juan, M. Clemente-León, E. Coronado, *Dalton Trans.* **2021**, *50*, 5931.

[90] A. Świtlicka, B. Machura, M. Penkala, A. Bieńko, D. C. Bieńko, J. Titiš, C. Rajnák, R. Boča, A. Ozarowski, *Inorg. Chem. Front.* **2020**, *7*, 2637.

[91] J. Li, Y. Han, F. Cao, R.-M. Wei, Y.-Q. Zhang, Y. Song, *Dalton Trans.* **2016**, *45*, 9279.

[92] D. Shao, P. Peng, M. You, L.-F. Shen, S.-Y. She, Y.-Q. Zhang, Z. Tian, *Inorg. Chem.* **2022**, *61*, 3754.

[93] J. Vallejo, M. Viciano-Chumillas, F. Lloret, M. Julve, I. Castro, J. Krzystek, M. Ozerov, D. Armentano, G. D. Munno, J. Cano, *Inorg. Chem.* **2019**, *58*, 15726.

[94] I. Nemec, R. Herchel, Z. Trávníček, *Dalton Trans.* **2018**, *47*, 1614.

[95] R. Ishikawa, Y. Horii, R. Nakanishi, S. Ueno, B. K. Breedlove, M. Yamashita, S. Kawata, *Eur. J. Inorg. Chem.* **2016**, *20*, 3233.

[96] Y. Wu, D. Tian, J. Ferrando-Soria, J. Cano, L. Yin, Z. Ouyang, Z. Wang, S. Luo, X. Liu, E. Pardo, *Inorg. Chem. Front.* **2019**, *6*, 848.

[97] C. Plenk, J. Krause, E. Rentschler, *Eur. J. Inorg. Chem.* **2015**, *3*, 370.

[98] Y. Peng, V. Mereacre, C. E. Anson, Y. Zhang, T. Bodenstein, K. Fink, A. K. Powell, *Inorg. Chem.* **2017**, *56*, 6056.

[99] N. Plyuta, S. Petrusenko, V. N. Kokozay, T. Cauchy, F. Lloret, M. Julve, J. Cano, N. Avarvari, *Dalton Trans.* **2022**, *51*, 4760

[100] R. Boča, C. Rajnák, J. Moncol, J. Titiš, D. Valigura, *Inorg. Chem.* **2018**, *57*, 14314.

[101] D. Valigura, C. Rajnák, J. Moncol, J. Titiš, R. Boča, *Dalton Trans.* **2017**, *46*, 10950.

[102] C. Rajnák, J. Titiš, J. Moncol', R. Boča, *Dalton Trans.* **2020**, *49*, 4206.

[103] Y. F. Deng, M. K. Singh, D. Gan, T. Xiao, Y. Wang, S. Liu, Z. Wang, Z. Ouyang, Y. Z. Zhang, K. R. Dunbar, *Inorg. Chem.* **2020**, *59*, 7622.

[104] A. K. Kharwar, A. Mondal, S. Konar, *Dalton Trans.* **2021**, *50*, 2832.

[105] J. Zhou, J. Song, A. Yuan, Z. Wang, L. Chen, Z. W. Ouyang, *Inorg. Chim. Acta* **2018**, *479*,113.

[106] A. V. Palii, D. V. Korchagin, E. A. Yureva, A. V. Akimov, E. Y. Misochko, G. V. Shilov, A. D. Talantsev, R. B. Morgunov, S. M. Aldoshin, B. S. Tsukerblat, *Inorg. Chem.* **2016**, *55*, 9696.

[107] S. Y. Chen, H. H. Cui, Y. Q. Zhang, Z. Wang, Z. W. Ouyang, L. Chen, X. T. Chen, H. Yan, Z. L. Xue, *Dalton Trans.* **2018**, *47*, 10162.

[108] R. Sato, K. Suzuki, T. Minato, M. Shinoe, K. Yamaguchi, N. Mizuno, *Chem. Commun.* **2015**, *51*, 4081.

[109] P. K. Sahu, A. Mondal, S. Konar, *Dalton Trans.* **2021**, *50*, 3825.

[110] P. Happ, C. Plenk, E. Rentschler, *Coord. Chem. Rev.* **2015**, *289*, 238.

[111] M. A. Palacios, J. Nehrkorn, E. A. Suturina, E. Ruiz, S. Gómez-Coca, K. Holldack, A. Schnegg, J. Krzystek, J. M. Moreno, E. Colacio, *Chem. Eur. J.* **2017**, *23*, 11649.

[112] J. Acharya, A. Swain, A. Chakraborty, V. Kumar, P. Kumar, J. F. Gonzalez, O. Cador, F. Pointillart, G. Rajaraman, V. Chandrasekhar, *Inorg. Chem.* **2019**, *58*, 10725.

[113] V. Chandrasekhar, A. Dey, A. J. Mota, E. Colacio, *Inorg. Chem.* **2013**, *52*, 4554.

[114] J. Palion-Gazda, T. Klemens, B. Machura, J. Vallejo, F. Lloret, M. Julve, *Dalton Trans.* **2015**, *44*, 2989.

[115] J. Vallejo, F. R. Fortea-Pérez, E. Pardo, S. Benmansour, I. Castro, J. Krzystek, D. Armentano, J. Cano, *Chem. Sci.* **2016**, *7*, 2286.

[116] Y. Y. Zhu, M. S. Zhu, T. T. Yin, Y. S. Meng, Z. Q. Wu, Y. Q. Zhang, S. Gao, *Inorg. Chem.* **2015**, *54*, 3716.

[117] L. Sun, S. Zhang, S. Chen, B. Yin, Y. Sun, Z. Wang, Z. Ouyang, J. Ren, W. Wang, Q. Wei, G. Xie, S. Gao, *J. Mater. Chem. C* **2016**, *4*, 7798.

[118] A. K. Mondal, S. Khatua, K. Tomar, S. Konar, *Eur. J. Inorg. Chem.* **2016**, *2016*, 3545.

[119] X. Liu, L. Sun, H. Zhou, P. Cen, X. Jin, G. Xie, S. Chen, Q. Hu, *Inorg. Chem.* **2015**, *54*, 8884.

[120] Y. L. Wang, L. Chen, C. M. Liu, Y. Q. Zhang, S. G. Yin, Q. Y. Liu, *Inorg. Chem.* **2015**, *54*, 11362.

[121] X. Liu, X. Ma, P. Cen, F. An, Z. Wang, W. Song, Y.-Q. Zhang, *New J. Chem.* **2018**, *42*, 9612.

[122] D. Ma, G. Peng, Y. Y. Zhang, B. Li, *Dalton Trans.* **2019**, *48*, 15529.

[123] J. M. Zadrozny, J. Liu, N. A. Piro, C. J. Chang, S. Hill, J. R. Long, *Chem. Commun.* **2012**, *48*, 3927.

[124] L. Tesi, A. Lunghi, M. Atzori, E. Lucaccini, L. Sorace, F. Totti, R. Sessoli, *Dalton. Trans.* **2016**, *45*, 16635.

Entry for the Table of Contents

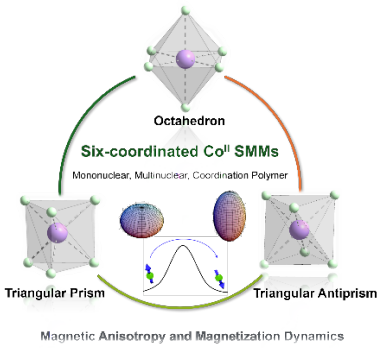

In this review, we summarize the progress in six-coordinated Co^{II} single-molecule magnets (SMMs), including mononuclear complexes, multinuclear complexes, and coordination polymers. The coordination geometry of the Co^{II} ion varies from octahedrons and triangular prisms to triangular antiprisms, which gives rise to distinct magnetic anisotropy and magnetization dynamics. The insights gathered from this review offer valuable guidance for future optimization.